Available online at www.sciencedirect.com
ScienceDirect
Surface & Coatings Technology 202 (2008) 4011–4018
SURFACE & COATINGS TECHNOLOGY
www.elsevier.com/locate/surfcoat

Tribological behaviour of titanium carbide/amorphous carbon nanocomposite coatings: From macro to the micro-scale

J.C. Sánchez-López *, D. Martínez-Martínez [1], C. López-Cartes, A. Fernández

Instituto de Ciencia de Materiales de Sevilla, CSIC-Universidad de Sevilla, Avda. Américo Vespucio 49, 41092-Sevilla, Spain

Received 1 October 2007; accepted 12 February 2008
Available online 10 March 2008

Abstract

The tribological behaviour of nanocomposite coatings made of nanocrystalline metal carbides and amorphous carbon (a-C) prepared by PVD/CVD techniques is found to be very dependant on the film deposition technique, synthesis conditions and testing parameters. Focusing in the TiC/amorphous carbon-based nanostructured system, this paper is devoted to an assessment of the factors governing the tribological performance of this family of nanocomposites using a series of TiC/a-C films prepared by magnetron sputtering technique varying the power applied to each target (titanium or graphite) as model system to establish correlations between film microstructure and chemical compositions and tribological properties measured by a pin-on-disk tribometer. The film microstructure goes from a quasi-polycrystalline TiC to a nanocomposite formed by nanocrystals of TiC embedded in an amorphous carbon matrix as observed by transmission electron microscopy (TEM). The nanocrystalline/amorphous ratio appears to be the key-parameter to control the tribological properties and its quantification has been done by electron energy-loss spectroscopy (EELS). A significant change in the tribological performance is observed for nanocomposites with amorphous carbon phase contents above 60–65%. The friction coefficient decreases from 0.3 to 0.1 and the film wear rates by a factor of 10. Examination of the wear scars on ball and film surfaces by laser micro-Raman spectroscopy has allowed to determine the presence of metallic oxides and carbonaceous compounds responsible of the observed friction behaviour. The revision of the literature results in view of the conclusions obtained enabled to explain their apparent dispersion in the tribological performance.

Keywords: Nanocomposites; Wear; Tribology; Friction; a-C; TiC

1. Introduction

The development of multilayered and nanocomposite heterostructures allows tailoring material properties to a specific desired value by superlattice and grain size effects. In the field of protective coatings, superior mechanical properties have been reported in the last decade for systems combining various transition metal nitrides in nanostructured form (e.g. nc-TiN/a-Si_3N_4, nc-TiN/a-Si_3N_4/a- and nc-$TiSi_2$, nc-$(Ti_{1-x}Al_x)N$/a-Si_3N_4, nc-TiN/TiB_2, nc-TiN/BN, etc. [1–9]) displaying hardness values ranging from 40 to 60 GPa with excellent thermal resistance. These materials are excellent candidates for protective applications as cutting or drilling tools; however, for tribological applications other properties as low friction, wear resistance, toughness or load capacity are also needed in order to prevent the brittle fracture or delamination of the coating under severe conditions. One way to improve composite toughness is to combine the hard nanocrystalline phase with a soft matrix as TiC/a-C [10], ZrN/Cu [11] or ZrO_2/Cu [12]. This design maintains the crystallite size of the hard phase at the nanometric level (5–20 nm) to guarantee hardness separated by a second soft phase of several tens of nm of thickness that provides ductility. This configuration shows a large volume of grain boundaries which restricts initial crack sizes and helps to deflect and terminate growing cracks. Also the presence of an amorphous boundary phase facilitates grain boundary sliding introducing ductility and preventing fracture under severe load conditions. If this soft matrix has good tribological properties we can obtain simultaneously a continuous supply of lubricant at the contact increasing the tribo-mechanical performance in dry lubricated conditions. Voevodin et al. (2000) prepared a

* Corresponding author. Tel.: +34 954 48 95 79; fax: +34 954 46 06 65.
E-mail address: jcslopez@icmse.csic.es (J.C. Sánchez-López).
[1] Current address: Université libre de Bruxelles, Chemicals and Materials Department, Faculty of Applied Science, CP165/63, avenue F.D. Roosevelt 50, 1050, Brussels.

0257-8972/$ - see front matter © 2008 Elsevier B.V. All rights reserved.
doi:10.1016/j.surfcoat.2008.02.012

TiC/DLC nanocomposite which showed a pseudoplastic behaviour when dragging its surface with a diamond tip of 0.2 mm radius loaded with 50 N (contact stress ~7 GPa) [13]. Also, the observation of the cracks by high resolution scanning electron microscopy revealed that sliding cavitation were maintained in the nanometric regime due to the reduced size of the grains and enhanced mobility of boundaries. Many groups have later synthesised TiC/C tough composites for tribological applications [14–20] although the correlation of the friction properties with their chemical composition is quite unclear. Thus, for instance, Gulbinski et al. [15] finds friction a variation from 0.6 to 0.1 when total carbon content increases with a plateau around 0.45 for medium contents. Stuber and co-workers [16] sees no differences between TiC/C composites prepared with carbon content of 30 or 50% (average friction ~0.45) while a sample with a ratio 70%(TiC):30%(C) exhibits value below 0.1. Other authors expressed the friction values as a function of the titanium content [17,18]. It is observed that friction below 0.3 are achieved when at. Ti % is below 45. Higher incorporation of titanium led to a sharp increase to 0.6 mean values. This lack of correlation could be partially attributed to the employment of different deposition techniques and synthesis conditions together with the difficulties inherent to the evaluation of tribological properties which are controlled by a nonlinear interaction of several different parameters. Also, the different way of displaying the friction properties in respect to the chemical composition does not help to compare the data among different works. The main motivation of this paper is to understand the tribological behaviour of this type of nanocomposites by the establishment of correlation between phase composition, film microstructure and tribological properties. To achieve this goal a family of TiC/a-C coatings has been prepared by magnetron sputtering with controlled chemical composition and microstructure that serves as base material to propose a friction mechanism that can be extrapolated to explain the reported literature data.

2. Experimental details

TiC/a-C nanocomposite coatings were prepared by Ar^+ sputtering of Ti (Goodfellow, 99.99% purity) and graphite targets. The magnetron sources were d.c. (graphite) and r.f. (Ti) working at sputtering power ratios (SPR), defined as the ratio of sputtering power applied to graphite target in respect to Ti one, from 1 to 4. The pressure of the vacuum chamber was measured before deposition in 6.5×10^{-4} Pa and 0.75 Pa while growing. The substrate were mounted in a rotary sample-holder (10 rpm) to ensure homogeneity and the temperature was found to vary in the range of 150–200 °C under the effect of the plasma. No additional heating or biasing of the substrate was done. Further experimental details concerning the synthesis conditions can be found in reference [21]. The crystal structure of the films was examined by X-ray diffraction analysis (XRD) at a low incidence angle of 1° in order to increase the signal from the coating compared with the substrate. Transmission electron microscopy (TEM) observation of the samples coupled with electron energy-loss spectroscopy (EELS) analysis were carried out in a Philips CM200 microscope operating at 200 kV and equipped with a parallel detection EELS spectrometer from Gatan (766–2 kV). The C K-edge was recorded in the diffraction mode with a camera length of 470 mm and a 2 mm-spectrometer entrance aperture yielded an energy resolution at the zero-loss peak of 1.4 eV. Tribological tests were carried out using 6 mm-diameter 100Cr6 steel balls in a pin-on-disk CSM tribometer with a sliding speed of 10 cm/s and 5 N of applied load in ambient air (30–60% of relative humidity). Normalized wear rates of the coatings ($mm^3\ N^{-1}\ m^{-1}$) were evaluated from cross sectional profiles taken across the disk wear track after testing by means of stylus profilometry. Micro-Raman measurements were performed using a LabRAM Jobin Yvon spectrometer equipped with a microscope. Laser radiation ($\lambda=532$ nm) was used as excitation source at 5 mW. All measurements were recorded under the same conditions (10 s of integration time and 10 accumulations) using a 100× magnification objective and a 100 μm pinhole.

3. Results and discussion

In a previous work [21] we have shown the preparation of nc-TiC/a-C by changing the sputtering power ratio applied to two targets (carbon and titanium). Varying this parameter from 1 to 4 (i.e. SPR=4 means power applied to C target is four times that of Ti) we could obtain film microstructures going from densely packed crystals, with a thin separation among them, to small spherical grains randomly distributed in an amorphous

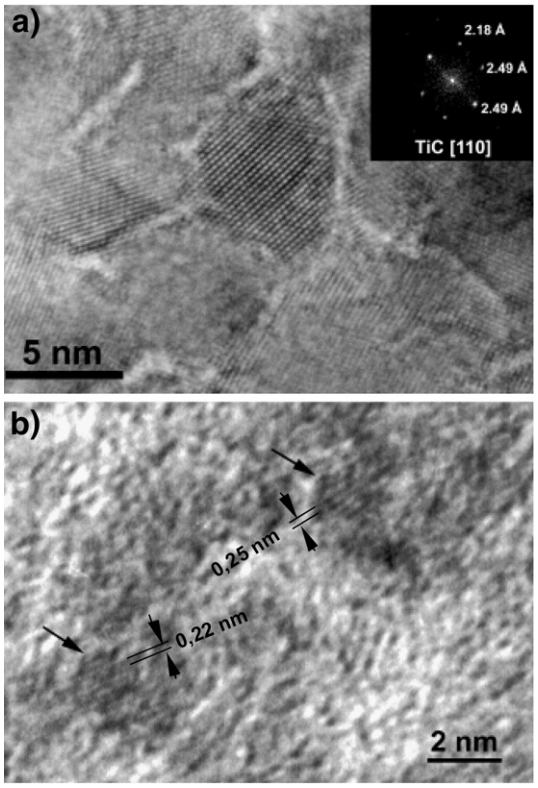

Fig. 1. HRTEM micrographs and corresponding electron diffraction patterns for nc-TiC/a-C nanocomposite coatings prepared at sputtering power ratios of 1 (a) and 4 (b) respectively.

Table 1
Summary of samples, phase contents and tribomechanical properties

Film	% TiC	% a-C	H (GPa)	f	K_{film} (10^{-7} mm^3/Nm)
A	15	85	8	0.13	1
B	21	79	7	0.12	6.8
C	23	77	7	0.10	2.3
D	25	75	7	0.09	2.6
E	30	70	16	0.10	2.7
F	45	55	18	0.26	52.6
G	47	53	27	0.25	25.6
H	90	10	16	0.25	44.4
I	95	5	22	0.31	47.5
J	>100*	0	11	0.6	60.8

* See text for explanation.

matrix. Fig. 1a and b displays two representative HRTEM images obtained from films prepared at SPRs 1 and 4 respectively. The sample prepared at with SPR = 1 (Fig. 1a) is formed by crystals of 5–10 nm with random orientation. The diffraction pattern shown as inset in the figure was obtained by performing fast Fourier transformation from the grain located in the centre of the micrograph and corresponds to a TiC crystal oriented along [110] direction. In Fig. 1b, it is marked the position of two very small particles, around 1 nm in size, completely embedded in the amorphous matrix. Lattice fringes corresponding to crystalline TiC structure with d-spacings of 2.15 and 2.50 Å can be measured. In this case the amorphous phase to crystalline phase ratio is clearly increased in respect to the previous film. The nanocomposite character and the combination of different phases into its structure were further confirmed by lateral force microscopy (LFM). The application of this approach was illustrated in reference [22] to demonstrate a texture formed by round agglomerates separated by a boundary region whose friction properties were different.

If we are interested to correlate the synthesis conditions, chemical composition and phases proportion inside the film the application of other techniques providing chemical information is needed. In this case, the measurement of the EELS spectra on the C K-edge core loss has enabled the estimation of the

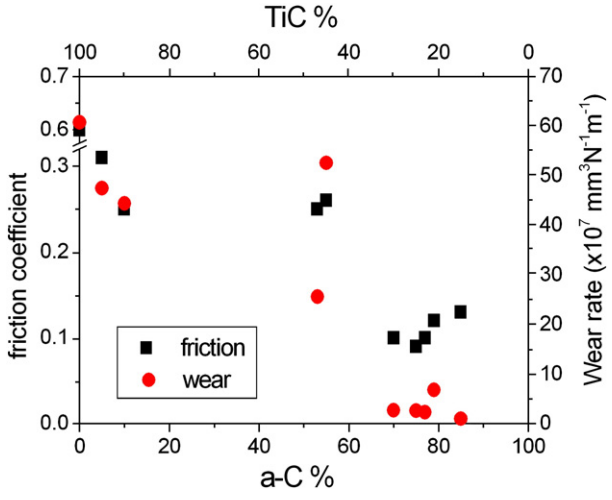

Fig. 2. Friction coefficients and wear rate values for nc-TiC/a-C nanocomposite coatings as a function of the a-C (TiC) contents in %.

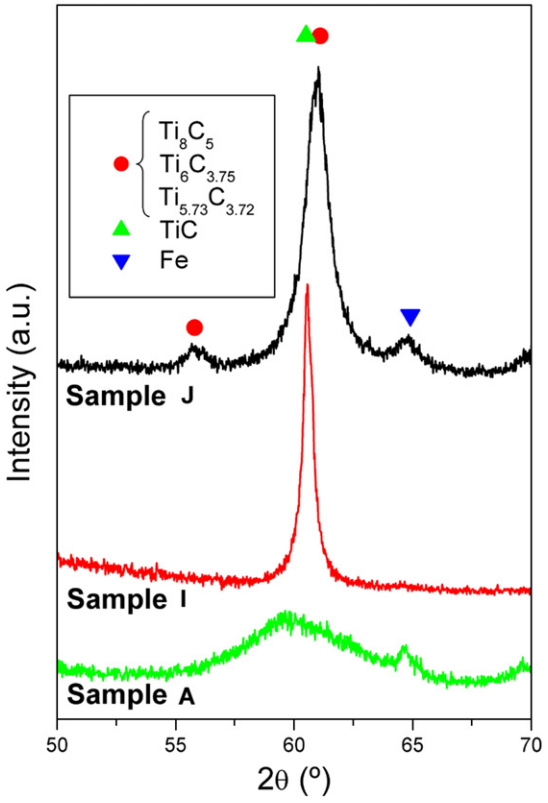

Fig. 3. XRD diffractograms for films A, I and J as representative examples of different type of friction behaviour (zoom 2Θ 50–70°). The database numbers for the identified crystalline phases are the following: TiC phase (database no. 32-1383), Ti_8C_5 (database no. 72-2496), $Ti_6C_{3.65}$ (database no. 79-0971) and $Ti_{5.73}C_{3.72}$ (database no. 77-1089).

amorphous C in the nanocomposite by comparing the near-edge fine structure of C K-edge electron energy-loss with two references of pure TiC and a-C respectively [21,23]. The shape and position of the spectra for the different nanocomposites changed gradually from those characteristics of a TiC to those of a-C phases. In fact, by using linear combinations between the reference spectra, we have estimated the TiC and a-C contents inside the nanocomposite. Table 1 collects the TiC contents ranging from 15 to 95% for the series of TiC/a-C

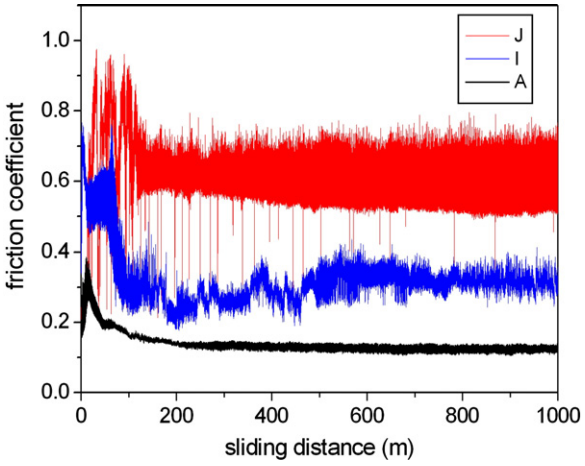

Fig. 4. Friction curves for TiC/a-C coatings (A, I and J).

nanocomposite coatings under study. A particular situation occurs in the EELS analysis of Sample J whose fitting analysis was not possible by using a TiC spectrum as reference [23]. This was attributed to the presence of a TiC phase rich in titanium as could be inferred from a Ti/C ratio measured by quantitative EELS of 1.9 and further confirmed by XRD, as will be shown lately. These estimations, which are in good agreement with the atomic chemical composition [21], demonstrates that the amorphous carbon contents can be tuned with the SPR parameter.

Considering the calculated a-C contents inside the coatings, we can analyze the dependence of the tribological properties as a function of this parameter. This representation is shown in Fig. 2 where a sharp transition in tribological behaviour is observed from (f~0.3, $K>10^{-6}$ mm^3/Nm) to ($f<0.2$, K: 10^{-7} mm^3/Nm) for amorphous carbon contents <55 and >70%, respectively. Additionally, it is observed a high degree of correlation between wear resistance and friction coefficient. The best tribological performance is obtained for the highest a-C contents even though the coating hardness decreases as a consequence of the major contribution of the soft matrix phase. However, the wear rate of the coatings appears thereby more influenced by the presence of the lubricant a-C matrix rather than hardness in accordance to what was highlighted in the introduction. The sample J is singular characterized by larger friction (0.6) and wear values along with a significant enrichment in titanium into its composition and therefore should be considered separately.

In order to investigate the reasons behind this different tribological behaviour, three samples A (85% a-C), I (5% a-C) and J (0% a-C) were selected for further analysis as representative example of each situation. Fig. 3 reproduces

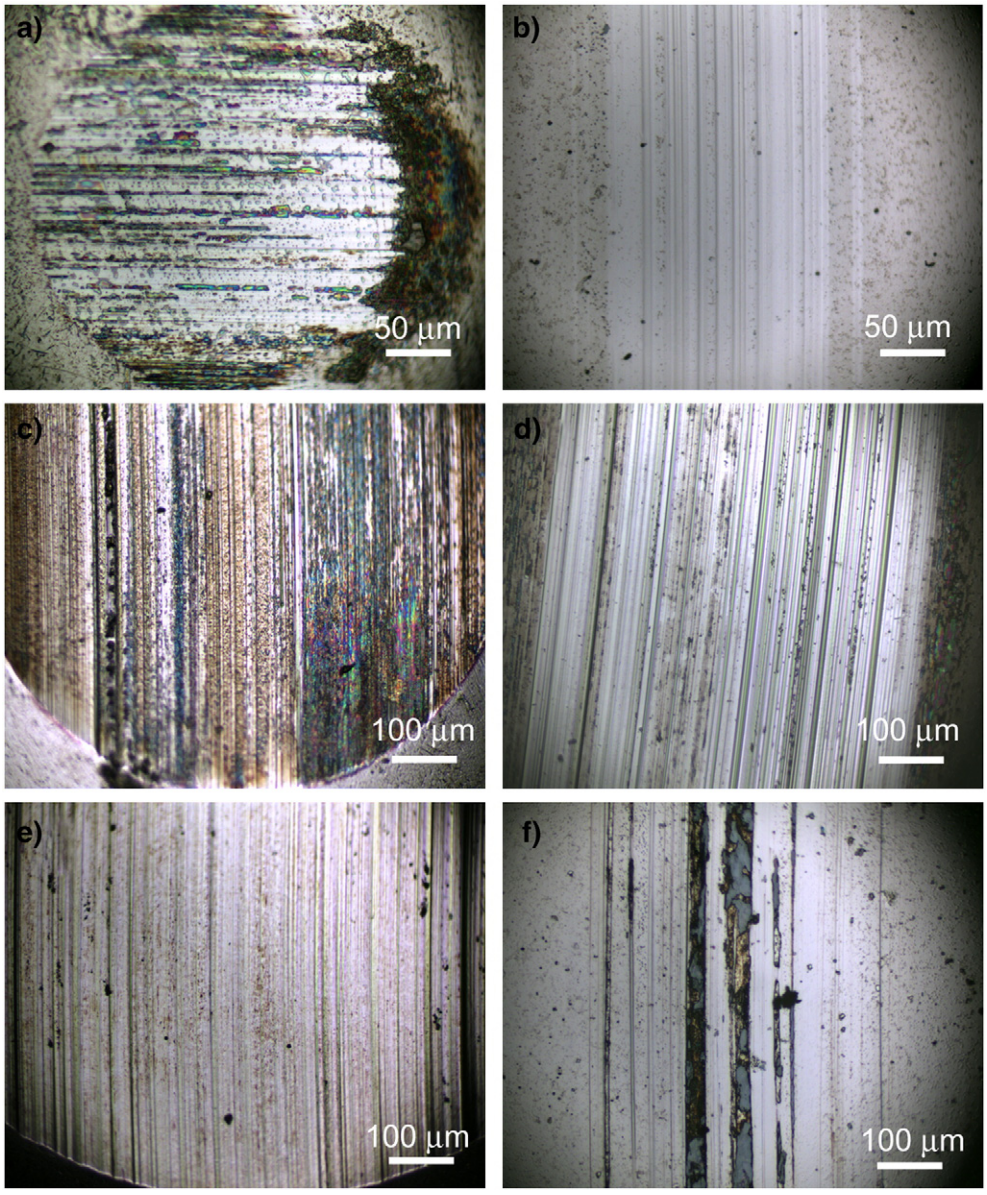

Fig. 5. Optical micrographs taken on the ball scars and wear track after friction testing of sample A (a, b); sample I (c, d) and sample J (e, f). Notice that double magnification was employed for the observation of counterfaces in coating C.

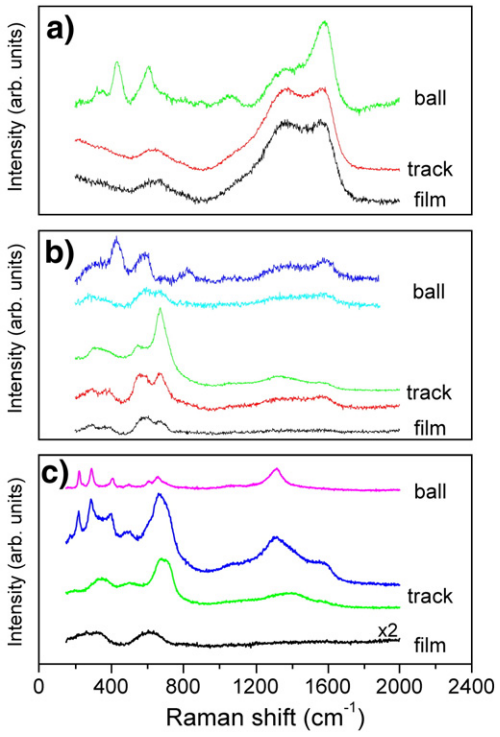

Fig. 6. Raman analysis of the worn surfaces (ball and coating) displayed in Fig. 4. Raman spectra for the initial coatings are included for comparison: sample A (a); sample I (b): sample J (c).

the XRD diffractograms for these aforementioned coatings. The diffraction patterns can be matched to cubic TiC phase (database no. 32-1383) whose crystal size is strongly reduced as the carbon content increases 5 to 85%. In the Sample J, a new contribution at 55.8° and substantial broadening of the (220) planes of TiC is attributed to the formation of non-stoichiometric Ti-enriched TiC phases (Ti_8C_5, $Ti_6C_{3.75}$, $Ti_{5.73}C_{3.72}$). These phases respond to a general empirical formula of $Ti_{1.6}C$. This result further confirms the conclusions obtained by EELS for this particular sample.

Fig. 4 displays the variation of the friction coefficient during a tribological test for samples A, I and J. The friction curves are characterized by a running period of around 100 m of higher friction followed by a decrease up to steady-state values. It should be noted that the friction coefficient is not only incremented at lower a-C %, but also the standard deviation and instability. With the aim of elucidating the tribochemical processes appearing at the contact region during friction, optical observation of the counterfaces coupled with Raman microanalysis was carried out.

Fig. 5 shows the optical micrographs for the wear scar on the ball and the film surfaces. Sample A (Fig. 5a and b) exhibits the smallest wear tracks in accordance with the lowest friction and wear experimented. The presence of wear debris and transferred layer onto the ball scar is also detected. Sample I exhibits a ball surface covered by coloured deposits and clear grooves on the film track. Finally, sample J (Fig. 5e and f) shows very worn surfaces with thick black deposits filling the film wear grooves. The Raman spectra obtained from these counterfaces are shown in the next figure (Fig. 6a, b and c) corresponding to samples A, I and J respectively. The Raman spectra measured for the as-deposited films are included for their comparison. Several spectra corresponding to a particular counterface are displayed when significant differences are encountered. The main phases detected by this analysis are summarized in Table 2. It should be noticed that initially only sample A exhibits the two bands at about 1370 (D-peak) and 1565 cm^{-1} (G-peak) characteristic of the sp^2 sites of all disordered carbons. This is in agreement with the higher carbon content in its film composition, in opposition to the other samples predominantly formed by TiC phases. Moreover, in these coatings some peaks are detected in the range of 450–750 cm^{-1}. These vibrational modes are indicative of understoichiometric titanium carbide. It should be mentioned that stoichiometric TiC has no Raman vibration modes but the introduction of disorder due to carbon vacancies makes them active [24,25]. Once the friction test proceeds different tribochemical reactions are induced producing noticeable modifications of the Raman spectra measured in the wear scars on ball and film. Thus, sample A still shows typical D and G bands in all spectra taken in the surfaces in contact during friction tests although the G-peak is enhanced and its position shifted to higher wavenumbers (1580 cm^{-1}) in the spectrum taken from the transfer material on the ball. These changes can be indicative of an ordering of an initial highly disordered sp^2-bonded C network (sputtered a-C) by reduction of defects [26]. Some features at 435 and 610 cm^{-1} are observed in the ball scar and debris that can be attributed to titanium oxides and/or iron titanate ($FeTiO_3$) [27]. The presence of this sp^2 carbon material on the surfaces provides easy-shear and low friction properties for this coating as commonly observed in the tribological behaviour of DLC coatings [28]. In the remaining samples I and J although some broad peaks in the region of disordered C are observed, their relevance is minor versus other peaks in the low wavenumber region that we analyzed hereafter in detail. In the wear track corresponding to sample I, we observed regions whose spectrum appears very similar to the original one along with other zones where the spectrum exhibits the typical pattern of iron oxide (magnetite) characterized by the dominance of A_{1g} mode at 666 cm^{-1} with a shoulder at 541 cm^{-1} [29,30]. In the ball scar we found either material transferred from the film to the mating surface whose spectrum looks almost unchanged (coloured transfer layer) along with partial oxidation of TiC phase. This chemical transformation is concluded by the development of peaks at approximately 430 and 600 cm^{-1} typical of titanium oxide and broad bands in the D–G region indicative of residual C that appears clearly insufficient to

Table 2
Summary of main phases detected on the counterfaces after friction testing of samples A, I and J

	Raman analysis		
	Film	Track	Ball
Sample A	a-C	a-C	a-C, nc-graphite + $FeTiO_3/TiO_x$
Sample I	TiC_x	$TiC_x + Fe_3O_4$ + a-C (small)	$TiC_x + TiO_x$ + a-C (small)
Sample J	TiC_x	α-$Fe_2O_3 + Fe_3O_4 + \gamma$-$Fe_2O_3$	α-Fe_2O_3

Table 3
Experimental conditions used for the friction tests in the reviewed references

Reference	Tribological testing						
	Ball		Conditions				
	Material	Diameter (mm)	Humidity (%)	T (°C)	Load (N)	Linear speed (cm/s)	Sliding distance
Feng [18]	WC-Co	4	40±20	r.t.	1	8.3–13.3	Minimum after 20 min
Gulbinski [15]	Al_2O_3	8	50	r.t.	1	–	–
Zhang [14]	100Cr6	6	75	22	10	20	–
Stuber [16]	100Cr6	6	25–50	23	1, 10	3, 15	1000 m
Zehnder [17]	100Cr6	6	60	–	5	10	700 m
Voevodin [20]	Steel	–	50±10	22	10	10	1000 m
Hu [19]	GCr15	3	50	r.t.	3	50	30 min (900 m)
This work	100Cr6	6	30–60	r.t.	5	10	1000 m

lubricate the contact region. Finally, the sample J exhibits more complex situation with multiple peaks in the region of 200 to 500 cm^{-1}. These new peaks, situated at 224, 289, 400 and 498 cm^{-1}, match quite well with those observed in iron oxide (hematite) and appear mixed with other iron oxides phases (maghemite/magnetite) whose main peak at 670/710 cm^{-1} is also present [29]. The origin of these peaks can be attributed to the formation of iron oxide by tribochemical reaction of the steel ball with the surrounding atmosphere under high friction conditions observed in this test. Another peculiarity observed in this sample is the appearance of an additional intense band at 1318 cm^{-1}. This peak has been shown to be an overtone (second order) of a first-order phonon band from α-Fe_2O_3 phase [30,31].

Consequently, the differences in tribological response for the aforementioned coatings can be correlated with the occurrence of different chemical reactions in the contact induced by the friction mechanism. Therefore, only when the amorphous carbon content inside the nanocomposite composition is sufficient, the contact appears covered by disordered sp^2-carbon material that helps to accommodate sliding motion and prevent the surfaces from mechanical wear and oxidation. This result is similar to that obtained with amorphous hydrogenated carbon/titanium carbide coatings [32–35]. When the coatings composition is dominated by TiC species, the friction increases appreciably and exchange of material is produced between both surfaces. When the coating is even enriched in titanium content these processes are enhanced due to higher adhesion between mating surfaces. As these phenomena proceed in ambient air, the formation of titanium and iron oxide phases corresponding to the oxidation of the film and ball counterfaces respectively is promoted. According to Fig. 2 the switch between these two friction regimes (carbon-lubricated and unlubricated) occurs for amorphous C contents between 55 to 70%.

To further confirm this friction behaviour we have extracted friction values from the literature for TiC/a-C(H) nanocomposites and plotted against the chemical composition. The experimental conditions used for the friction tests in the reviewed references are collected in Table 3. They are pin-on-

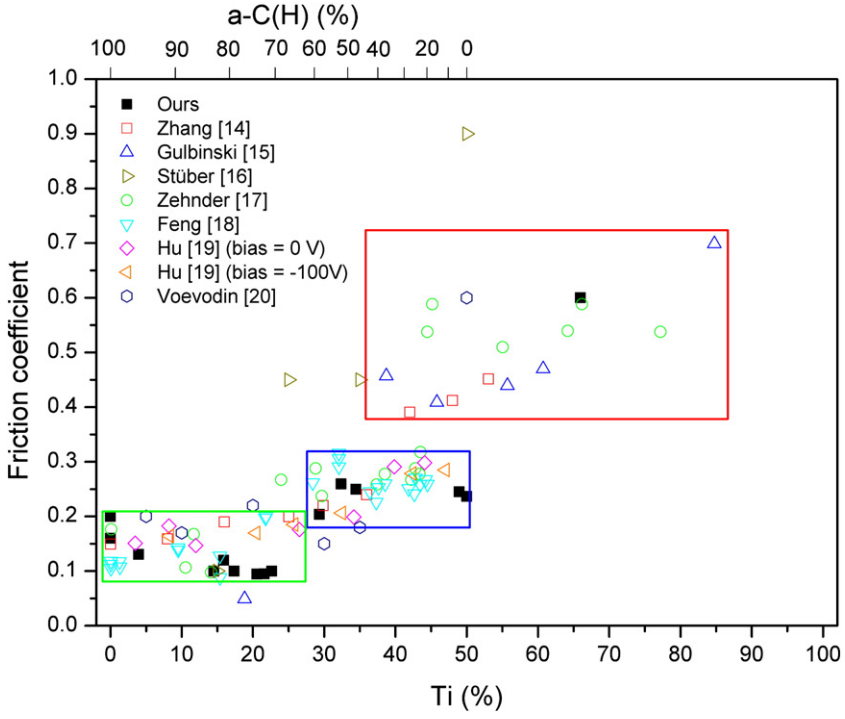

Fig. 7. Compilation of friction coefficient data reported in the literature for nc-TiC/a-C(H) nanocomposite coatings. The three different regions that can be distinguished are marked with rectangles.

disk experiments run in ambient air using mainly steel balls under different linear speed, applied load and counterball nature. Despite of the variety in these parameters in principle they can be considered altogether for their comparison with our data. The friction comparison is shown in Fig. 7. Three regions can be distinguished depending on the amount of Ti and the observed friction coefficient. Below ~30% Ti (i.e., >60% a-C) the samples show small values of friction coefficient, between 0.1 and 0.2. Over this limit and up to 50% Ti, a second group is found where the friction increases up to 0.3 and no samples with friction coefficient close to 0.1 are present. For high values of Ti content (>40%), samples with friction coefficient larger than 0.4 can be seen. As can be observed, the data assemble into three groups in agreement with the proposed friction regimes. Thanks to the increment in number of points in the first transition the interval found with our samples can now be reduced to a band around 60–65% a-C depending on type of film and testing conditions. This is rather significant taking into account the dispersion in tribological conditions, deposition procedure and approximate quantification of the lubricant phase. Most of the points for the coatings with carbon content less than this threshold remain in a range between 0.2–0.3 although higher values, up to 0.6, can appear. When the concentration of titanium approaches 50%, the friction values show a marked trend to increase up to 0.6 or higher [16]. This is probably due to the presence of Ti-rich compounds (Ti_xC with $x>1$) as was observed in sample J or even metallic Ti [13,15,17,36,37]. The increment of metallic character could be at the origin of this second friction rising influenced by adhesive wear mechanism and tribochemical oxidation phenomena at the contact. This analysis appear to confirm a general trend in the tribological behaviour of nanocrystalline/amorphous composites where the key-parameter is the ratio between the hard and the lubricant phase rather than hardness or the chemical composition itself without considering the phase and microstructure.

4. Conclusions

In this paper, the tribological behaviour of nanocomposite coatings made of crystalline TiC phase surrounded by an amorphous carbon-based matrix is reviewed by considering the ratio between these two phases as key-parameter controlling the friction and wear properties. Using a series of nc-TiC/a-C nanocomposite coatings with controlled microstructure and chemical composition prepared by magnetron sputtering as base system, different friction regimes were highlighted according to the film composition:

a) a-C lubricated (amorphous phase content >60–65%): tribological behaviour controlled by the presence of sp^2 disordered carbon which helps to accommodate the shear strength lubricating the contact; ($f<0.2$, K: 10^{-7} mm^3/Nm).

b) Unlubricated (amorphous phase content <60–65%):

b.1. (TiC): tribological behaviour is controlled by the TiC phase; ($f>0.2$ to 0.3, $K>10^{-6}$ mm^3/Nm) and characterized by the exchange of material and tribo-oxidation of both counterfaces.

b.2. (Ti/TiC): When the coating is even enriched in titanium content (at. %<50) these processes are enhanced due to higher adhesion between mating surfaces. This situation corresponds to understoichiometric TiC phases (TiC_x; $x<1$) or Ti-rich nanocomposites (Ti/TiC). Higher friction values (around 0.6), wear and oxidation are promoted.

This explanation was later validated by comparing with various data reported in the literature that were revised in terms of nanocrystalline/amorphous fractions. This a-C fraction threshold can be very useful for tailored design of self-lubricant nanocomposites and might anticipate the tribological response in practical applications.

Acknowledgement

Financial support from the Spanish MEC (project no. MAT2004-01052 and MAT2007-66881-C02-01) and the I3P program of CSIC is acknowledged.

References

[1] S. Veprek, M.G.J. Veprek-Heijman, P. Karvankova, J. Prochazka, Thin Solid Films 476 (2005) 1.
[2] S. Veprek, S. Reiprich, Sh. Li, Appl. Phys. Lett. 66 (1995) 2640.
[3] J. Musil, Surf. Coat. Technol. 125 (2000) 322.
[4] H.-D. Männling, D.S. Patil, K. Moto, M. Jilek, S. Veprek, Surf. Coat. Technol. 146–147 (2001) 263.
[5] L. Rebouta, U.C.J. Tavares, R. Aimo, Z. Wang, K. Pischow, E. Alves, T.C. Rojas, J.A. Odriozola, Surf. Coat. Technol. 133–134 (2000) 234.
[6] P. Holubar, M. Jilek, M. Sima, Surf. Coat. 133–134 (2000) 145.
[7] C. López-Cartes, D. Martínez-Martínez, J.C. Sánchez-López, A. Fernández, A. García-Luis, M. Brizuela, J.I. Oñate, Thin Solid Films 515 (2007) 3590.
[8] J.C. Sánchez-López, D. Martínez-Martínez, C. López-Cartes, A. Fernández, M. Brizuela, A. García-Luis, J.I. Oñate, J. Vac. Sci. Technol. A 23 (2005) 681.
[9] J. Patscheider, T. Zehnder, M. Diserens, Surf. Coat. Technol. 146–147 (2001) 201.
[10] A.A. Voevodin, S.V. Prasad, J.S. Zabinski, J. Appl. Phys. 82 (1997) 855.
[11] J. Musil, P. Zeman, Vacuum 52 (1999) 269–275.
[12] S. Lang, T. Beck, A. Schattke, C. Uhlaq, A. Dinia, Surf. Coat. Technol. 180 –181 (2004) 85.
[13] A.A. Voevodin, J.S. Zabinski, Thin Solid Films 370 (2000) 223.
[14] S. Zhang, X.L. Bui, J. Jiang, X.M. Li, Surf. Coat. Technol. 198 (2005) 206.
[15] W. Gulbinski, S. Mathur, H. Shen, T. Suszko, A. Gilewicz, B. Warcholinski, Appl. Surf. Sci. 239 (2005) 302.
[16] M. Stuber, H. Leiste, S. Ulrich, H. Holleck, D. Schild, Surf. Coat. Technol. 150 (2002) 218.
[17] T. Zehnder, J. Patscheider, Surf. Coat. Technol. 133 (2000) 138.
[18] B. Feng, D.M. Cao, W.J. Meng, L.E. Rehn, P.M. Baldo, G.L. Doll, Thin Solid Films 398 (2001) 210.
[19] Y. Hu, L. Li, X. Cai, Q. Chen, P.K. Chu, Diamond Relat. Mater. 16 (2007) 181.
[20] A.A. Voevodin, C. Rebholz, J.M. Schneider, P. Stevenson, A. Matthews, Surf. Coat. Technol. 73 (1995) 185–197.
[21] D. Martínez-Martínez, C. López-Cartes, A. Justo, A. Fernández, J.C. Sánchez-López, A. García-Luis, M. Brizuela, J.I. Oñate, J. Vac. Sci. Technol., A 23 (2005) 1732.
[22] D. Martínez-Martínez, J.C. Sánchez-López, T.C. Rojas, A. Fernández, P. Eaton, M. Belin, Thin Solid Films 472 (2005) 64.
[23] J.C. Sánchez-López, D. Martínez-Martínez, C. López-Cartes, C. Fernández-Ramos, A. Fernández, Surf. Coat. Technol. 200 (2005) 40.
[24] J. Soldán, J. Musil, Vacuum 81 (2006) 531–538.
[25] B.H. Lohse, A. Calka, D. Wexler, J. Alloy.Compounds 434–435 (2007) 405–409.
[26] A.C. Ferrari, J. Robertson, Phys. Rev. B 61 (2000) 14095–14107.

[27] M. Gotic, M. Ivanda, S. Popovic, S. Music, A. Sekulic, A. Turkovic, K. Furic, J. Raman Spectroscopy 28 (1997) 555–558.
[28] A. Erdemir, C. Donnet (Eds.), Fundamentals and Applications, Springer, New York, 2008.
[29] Chamritski, Burns, J. Phys. Chem., B 109 (2005) 4965–4968.
[30] D. Bersani, P.P. Lottici, A. Montenero, J. Raman Spectrosc. 30 (1999) 355.
[31] K.F. McCarthy, Solid State Commun. 68 (1988) 799–802.
[32] W.J. Meng, R.C. Tittsworth, L.E. Rehn, Thin Solid Films 377–378 (2000) 222.
[33] D.M. Cao, B. Feng, W.J. Meng, L.E. Rehn, P.M. Baldo, M.M. Khonsari, Appl. Phys. Lett. 79 (2001).
[34] Y.T. Pei, D. Galvan, J.Th.M. De Hosson, Acta Mater. 53 (2005) 4505.
[35] Y.T. Pei, D. Galvan, J.Th.M. De Hosson, A. Cavaleiro, Surf. Coat. Technol. 198 (2005) 44.
[36] J.E. Sundgren, B.O. Johansson, S.E. Karlsson, H.T.G. Hentzell, Thin Solid Films 105 (1983) 367.
[37] T. Zehnder, P. Schwaller, F. Munnik, S. Mikhailov, J. Patscheider, J. Appl. Phys. 95 (2004) 4327.